

# Repurposing $^{11}\text{C}$ -PS13 for PET Imaging of Cyclooxygenase-1 in Ovarian Cancer Xenograft Mouse Models

Amanda J. Boyle<sup>1</sup>, Junchao Tong<sup>1</sup>, Sami S. Zoghbi<sup>2</sup>, Victor W. Pike<sup>2</sup>, Robert B. Innis<sup>2</sup>, and Neil Vasdev<sup>1,3</sup>

<sup>1</sup>Azrieli Centre for Neuro-Radiochemistry, Brain Health Imaging Centre, Centre for Addiction and Mental Health, Toronto, Ontario, Canada; <sup>2</sup>National Institute of Mental Health, Bethesda, Maryland; and <sup>3</sup>Department of Psychiatry, University of Toronto, Toronto, Ontario, Canada

Cyclooxygenase-1 (COX-1), a biomarker for neuroinflammation, is implicated in the progression and prognosis of ovarian cancer (OvCa). This study considered the repurposing of  $^{11}\text{C}$ -labeled 1,5-bis(4-methoxyphenyl)-3-(2,2,2-trifluoroethoxy)-1*H*-1,2,4-triazole ( $^{11}\text{C}$ -PS13), a COX-1 PET neuroimaging radiopharmaceutical, in OvCa xenograft mouse models. **Methods:**  $^{11}\text{C}$ -PS13 was evaluated in ICRscid mice with subcutaneous or intraperitoneal human OVCAR-3 OvCa xenografts by dynamic PET/MRI, ex vivo biodistribution, and radiometabolite analysis of plasma and tumor. **Results:** OVCAR-3 xenografts were well visualized with  $^{11}\text{C}$ -PS13 in xenograft mouse models. Time-activity curves revealed a steady accumulation of tumor radioactivity that plateaued from 40 to 60 min and was significantly reduced by pretreatment with ketoprofen ( $3.56 \pm 0.81$  and  $1.30 \pm 0.18$  percentage injected dose/g without and with pretreatment, respectively,  $P = 0.01$ ). Radiometabolite analysis showed that intact  $^{11}\text{C}$ -PS13 accounted for more than 80% of radioactivity in the tumor, with less than 20% in plasma, at 40 min after injection. **Conclusion:**  $^{11}\text{C}$ -PS13 shows promise for PET imaging of COX-1 in OvCa, and rapid translation for clinical cancer research should be considered.

**Key Words:** cyclooxygenase-1; ovarian cancer; repurposing; PET;  $^{11}\text{C}$ , COX-1

**J Nucl Med 2021; 62:665–668**

DOI: 10.2967/jnumed.120.249367

Ovarian cancer (OvCa) is the most lethal gynecologic cancer, accounting for 5% of all cancer-related deaths, because in 80% of patients the diagnosis is not made until the disease is advanced (1). Early detection of OvCa is desperately needed to improve patient outcomes, as cases diagnosed at an early stage have a 5-y survival rate of 93%, compared with the dire 17% for those diagnosed after the disease has metastasized (1). There are few PET radiopharmaceuticals for OvCa in a clinical setting. The most common,  $^{18}\text{F}$ -FDG, has downfalls such as false-negative results in early-stage OvCa and false-positive results when inflammatory comorbidities are present (2,3). Preclinical research is avidly pursuing novel PET biomarkers

such as receptor overexpression, cell proliferation, vasculature, and hypoxia (3–10).

In OvCa, cyclooxygenase-1 (COX-1) overexpression is associated with a poor prognosis, tumorigenesis, and tumor invasion (11–13). To our knowledge, the only COX-1–targeted PET imaging agent being explored in preclinical oncology research is  $^{18}\text{F}$ -labeled 3-(4-fluorophenyl)-5,5-dimethyl-4-(*p*-tolyl)furan-2(5*H*)-one ( $^{18}\text{F}$ -FDF; half-maximal inhibitory concentration [ $\text{IC}_{50}$ ], 220 nM) (14).  $^{11}\text{C}$ -labeled 1,5-bis(4-methoxyphenyl)-3-(2,2,2-trifluoroethoxy)-1*H*-1,2,4-triazole ( $^{11}\text{C}$ -PS13) is a COX-1–targeted PET radiopharmaceutical that is more than 200-fold more potent than  $^{18}\text{F}$ -FDF and has recently been translated for clinical neuroimaging research (15–18). This study explored the potential for repurposing  $^{11}\text{C}$ -PS13 in rodent models of OvCa via dynamic PET imaging, ex vivo biodistribution studies, and radiometabolite analysis.

## MATERIALS AND METHODS

A description of the radiochemical synthesis of  $^{11}\text{C}$ -PS13 is available in the supplemental materials, which are available at <http://jnm.snmjournals.org> (17,19).

### Tumor Xenograft Mouse Models

OVCAR-3 human OvCa cells (American Type Culture Collection) with high COX-1 expression (14) were cultured in RPMI 1640 medium supplemented with 20% fetal bovine serum (Gibco, Life Technologies), 1% penicillin/streptomycin (Sigma-Aldrich), and 0.01 mg/mL bovine insulin (Sigma-Aldrich). The cells were cultured in an atmosphere of 5%  $\text{CO}_2$  at 37°C. ICRscid mice (Taconic Biosciences) were inoculated subcutaneously on the right flank and imaged when tumors reached 0.75–1.0 cm in diameter, or they were inoculated intraperitoneally with  $1 \times 10^7$  OVCAR-3 cells in 100  $\mu\text{L}$  of phosphate-buffered saline combined with 100  $\mu\text{L}$  of Matrigel (Corning). Mice bearing intraperitoneal xenografts, which are more physiologically relevant than subcutaneous xenografts, were imaged sporadically from week 2 to week 6 after inoculation to examine the potential for  $^{11}\text{C}$ -PS13 to detect early-stage OvCa. Animal studies were conducted under protocol 817 approved by the Animal Care Committee at the Centre for Addiction and Mental Health, following Canadian Council on Animal Care guidelines. Male mice were used to generate subcutaneous models for preliminary PET imaging, whereas female mice were used to generate intraperitoneal and subcutaneous cancer models for PET imaging and radiometabolite analysis, respectively.

### PET/MRI and Biodistribution Studies

**PET Acquisition.** For small-animal PET combined with MRI, the mice were anesthetized by isoflurane in  $\text{O}_2$  (4%, 2 L/min induction; 1%–2%, 1 L/min maintenance) for lateral tail-vein catheterization and then transferred to a nanoScan PET/MRI 3-T scanner (Mediso). Six

Received May 11, 2020; revision accepted Aug. 17, 2020.

For correspondence or reprints contact: Neil Vasdev, Centre for Addiction and Mental Health, CAMH Research Imaging Center, 250 College St., Toronto, ON M5T1R8, Canada.

E-mail: [neil.vasdev@utoronto.ca](mailto:neil.vasdev@utoronto.ca)

Published online Sep. 25, 2020.

COPYRIGHT © 2021 by the Society of Nuclear Medicine and Molecular Imaging.

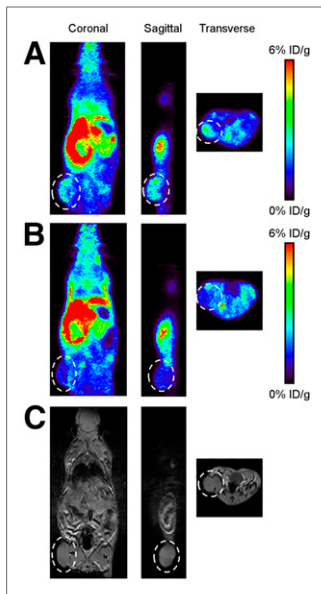


**FIGURE 1.** PET imaging of  $^{11}\text{C}$ -PS13 in OVCAR-3 subcutaneous xenograft mice. (A and B) Representative PET images of  $^{11}\text{C}$ -PS13 under baseline (A) and blocked (B) conditions. (C) Associated MR images for A and B. Tumors are encircled.

selected tissue samples were collected, weighed, and transferred to  $\gamma$ -counting tubes. Tissue radioactivity was measured with a  $\gamma$ -counter and expressed as %ID/g.

**PET Data Analysis.** Image analyses and extraction of time-activity curves in regions of interest were performed in Amide, version 1.0.4.

mice were injected through the tail-vein catheter with  $^{11}\text{C}$ -PS13 (2.00–9.93 MBq, 1.53–9.02 nmol/kg, 11–101 GBq/ $\mu\text{mol}$ ). Two mice were pretreated with an intraperitoneal injection of 2 mg of the COX-1 inhibitor, ketoprofen (Selleck Chemicals), in 20  $\mu\text{L}$  of dimethylsulfoxide 60 min before bolus injection of  $^{11}\text{C}$ -PS13.

With the mouse anesthetized and stable in the PET/MRI scanner, a short gradient-echo scout MRI was acquired for positioning the mouse in the PET field of view, followed by a T1-weighted material map MRI acquisition (a short gradient-echo 3-dimensional acquisition with a repetition time of 25 ms and an echo time of 4.76 ms) for PET and MRI coregistration and PET scatter and attenuation corrections. PET scans were initiated at the time of radioligand injection, and the list-mode data were acquired for 60 min with an energy window of 400–600 keV.

Biodistribution was performed on mice bearing subcutaneous xenografts. The mice were sacrificed by cervical dislocation, and

Acquired data were sorted into thirty-three 3-dimensional ( $3 \times 5 \text{ s}$ ,  $3 \times 15 \text{ s}$ ,  $3 \times 20 \text{ s}$ ,  $7 \times 60 \text{ s}$ ,  $17 \times 180 \text{ s}$ ) true sinograms (ring difference, 84). The 3-dimensional sinograms were converted in 2-dimensional sinograms using Fourier rebinning (20) with corrections for detector geometry, efficiencies, attenuation, and scatter, before image reconstruction using 2-dimensional filtered backprojection with a Hann filter at a cutoff of  $0.50 \text{ cm}^{-1}$ . A static image of the complete emission acquisition was reconstructed with the manufacturer's iterative 3-dimensional algorithm (6 subsets, 4 iterations). The static iterative image was used for PET and MRI coregistration and for presentation in figures. All data were corrected for dead time and were decay-corrected to the start of acquisition. Dynamic filtered backprojection images were used to extract time-activity curves. Regions of interest were placed in the tumor or contralateral muscle tissue. Time-activity curves were extracted from regions of interest and expressed as percentage injected dose (%ID)/g, assuming tissue density of 1 g/mL.

#### Radiometabolite Analysis

Tumor-bearing mice were sacrificed by cervical dislocation 40 min after injection with  $^{11}\text{C}$ -PS13 (16.84–22.54 MBq, 1.72–5.84 nmol/kg, 99.5–434 GBq/ $\mu\text{mol}$ ). Blood was collected by cardiac heart puncture and then centrifuged for 5 min at 1,500g. Tumors were excised and homogenized with a Polytron homogenizer (Kinematica) in 2 mL of acetonitrile with 50 ng of PS13 to improve extraction of  $^{11}\text{C}$ -PS13 from the tissue, and then 1 mL of  $\text{H}_2\text{O}$  was added. The homogenate was centrifuged at 13,500 g for 5 min.  $^{11}\text{C}$ -PS13 product, plasma, and tumor homogenates were separated by column-switching high-performance liquid chromatography, as previously described, with a mobile phase of acetonitrile in 0.1N (aqueous) ammonium formate (65:35 v/v) and analyzed with PowerChrom, version 2.6.15 (eDAQ) (21).

#### Statistical Analysis

Data are represented as the mean  $\pm$  SD. Statistical comparisons were performed by an unpaired *t* test, corrected for multiple comparisons using the Bonferroni–Dunn method ( $P < 0.05$ ) with GraphPad Prism, version 8.3.1.

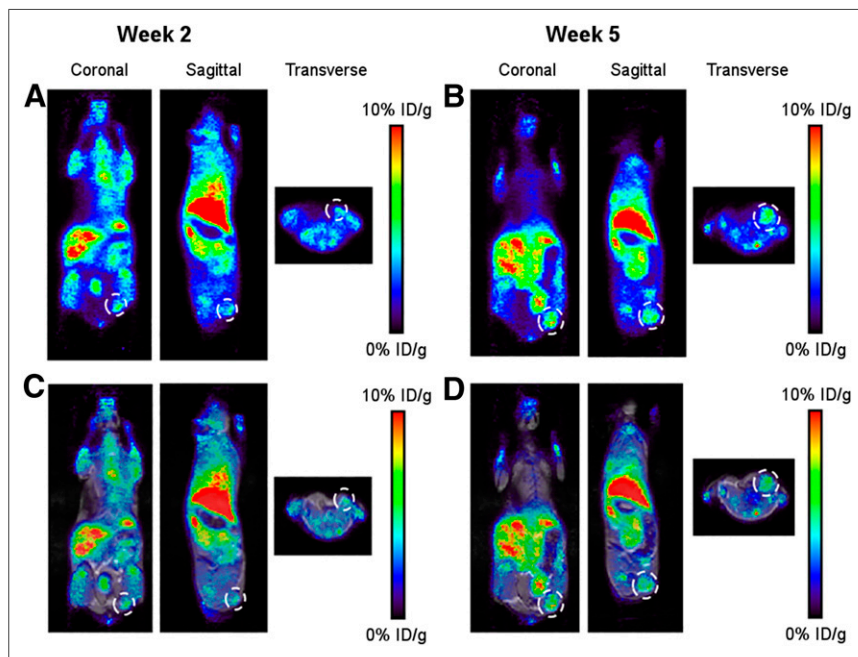


**FIGURE 2.** PET imaging of  $^{11}\text{C}$ -PS13 in OVCAR-3 intraperitoneal xenograft mouse model. PET images (A and B) and PET/MR images (C and D) were obtained at weeks 2 and 5 after inoculation with cancer cells. Tumors are encircled.

## RESULTS

### PET/MRI of OVCAR-3 Tumor-Bearing Mice

We evaluated  $^{11}\text{C}$ -PS13 in ICRScid mice bearing subcutaneous or intraperitoneal OVCAR-3 xenografts. Figure 1A shows representative static PET images in which tumors were visualized with  $^{11}\text{C}$ -PS13 (0- to 60-min average image). Figure 1B depicts representative PET images of tumor-bearing mice pretreated with ketoprofen, showing a reduced accumulation of tumor radioactivity, thus demonstrating the COX-1 specificity of  $^{11}\text{C}$ -PS13. Figure 2 shows representative static PET images in which intraperitoneal xenografts were visualized as early as 2 wk after inoculation with OVCAR-3 cells. Supplemental Figures 1 and 2 show PET imaging data in other intraperitoneal xenograft mice ( $n = 3$ ).

Time-activity curves revealed a steady accumulation of tumor radioactivity that plateaued from 40 to 60 min, with an average uptake of  $3.56 \pm 0.81 \text{ \%ID/g}$  ( $n = 6$ ) (Figs. 3A and 3B). Muscle tissue exhibited

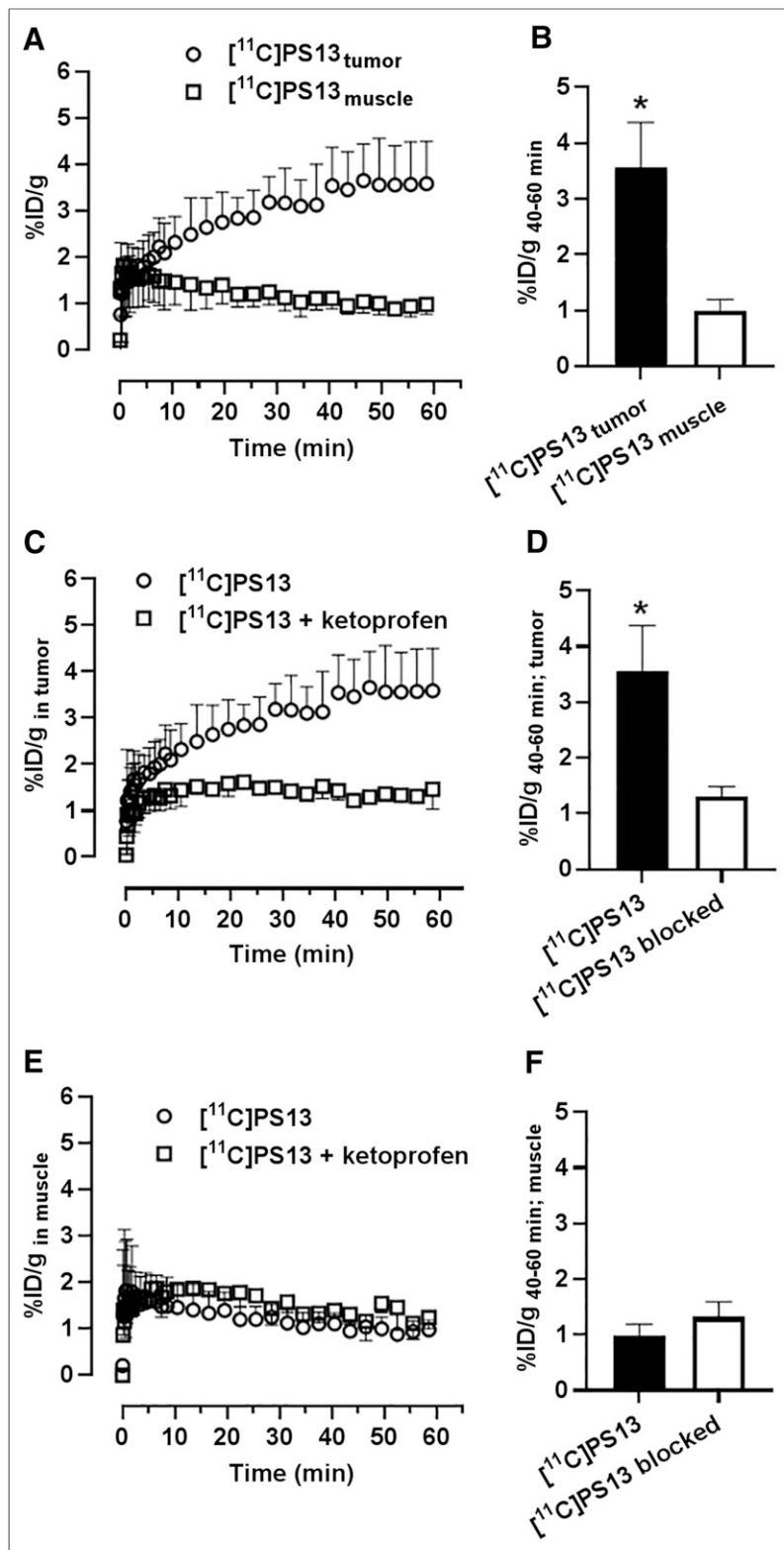


**FIGURE 3.** (A, C, and E) Time-activity curves of  $^{11}\text{C}$ -PS13 in tissues of OVCAR-3 subcutaneous xenograft mice over 60 min in tumor tissue and muscle tissue (A), tumor under baseline and blocked conditions (C), and muscle tissue under baseline and blocked conditions (E). (B, D, and F) Average uptake at 40-60 min in tumor and muscle tissue (B), tumor under baseline and blocked conditions (D), and muscle tissue under blocked and unblocked conditions (F). \*Significant differences.

washout of radioactivity over time, and the average uptake between 40 and 60 min was significantly lower than for tumor tissue ( $0.99 \pm 0.21$  %ID/g;  $P = 0.00002$ ), leading to a tumor-to-muscle ratio of 3.60 (Figs. 3A and 3B). The time-activity curves in Figure 3C show that the accumulation of radioactivity in tumors was significantly reduced (63.5%) by pretreatment with ketoprofen, to  $1.30 \pm 0.18$  %ID/g ( $P = 0.0096$ ). Pretreatment with ketoprofen did not affect muscle accumulation; therefore, off-target binding of  $^{11}\text{C}$ -PS13 was not apparent (Figs. 3E and 3F). PET imaging analyses were substantiated by ex vivo biodistribution studies (Supplemental Fig. 3; Supplemental Table 1). The average uptake from 40 to 60 min for intraperitoneal xenograft mice was  $4.78 \pm 0.88$  %ID/g.

#### Radiometabolite Analysis

The ex vivo composition of  $^{11}\text{C}$ -PS13 in plasma and tumor tissue was determined at 40 min after injection (based on the plateau in the time-activity curves) in subcutaneous tumor-bearing mice by high-performance liquid chromatography analysis of relative amounts of parent radioligand and radiometabolites. At 40 min after injection, intact  $^{11}\text{C}$ -PS13 represented  $17.5\% \pm 1.6\%$  of the total radioactivity in the plasma and  $80.6\% \pm 0.7\%$  in the tumor tissue (Supplemental Figs. 4 and 5). This analysis represents a single time-point in compartmental modeling of the tumor; future studies will examine complete compartmental modeling with various time points.

#### DISCUSSION

$^{11}\text{C}$ -PS13 is the most potent and selective COX-1 inhibitor reported to date and has recently been translated for human PET studies of neuroinflammation (16). Repurposing this PET radiopharmaceutical to OvCa imaging can greatly accelerate the timeline for translation of a COX-1 radiopharmaceutical for oncology (22). Herein, we report the successful PET/MR imaging of human OvCa xenografts with COX-1-targeted  $^{11}\text{C}$ -PS13, with a high accumulation of radioactivity in the tumor. Time-activity curves showed a desirable pharmacologic profile for  $^{11}\text{C}$ -PS13: radioactivity accumulated in the tumor while remaining low in muscle tissue and washed out over time (Fig. 3A).

Target-engagement experiments showed that COX-1 mediates  $^{11}\text{C}$ -PS13 accumulation in the tumor, with a 2.7-fold decrease observed in mice pretreated with ketoprofen (Fig. 3C). Our study demonstrated that

tumor accumulation of  $^{11}\text{C}$ -PS13 was 3-fold greater than that reported for  $^{18}\text{F}$ -FDF in a subcutaneous OvCa xenograft mouse model (14). We also demonstrated the potential for  $^{11}\text{C}$ -PS13 to detect early-stage OvCa in clinically relevant intraperitoneal xenograft mouse models, in which tumors were successfully visualized at 2 wk after inoculation (Fig. 2). Because tumor growth inhibition has been demonstrated by COX-1 inhibitors in preclinical studies (23), the radiometabolite analysis showing sequestering of intact  $^{11}\text{C}$ -PS13 in tumor tissue suggests that this radiotracer could potentially be useful for confirming target engagement and dosing regimens for nonradioactive COX-1 therapeutics in oncology. Notably,  $^{11}\text{C}$ -PS13 has a lower affinity for rodent COX-1 than for human COX-1 ( $\text{IC}_{50}$ , 15 and 1 nM, respectively). Despite this lower affinity, a difference in  $^{11}\text{C}$ -PS13 background between rodent and higher species is not expected because no specific binding of  $^{11}\text{C}$ -PS13 was observed in healthy ovarian tissue of rhesus monkeys (15), as is consistent with our preliminary human data (unpublished data, June 2020).

## CONCLUSION

We report the successful repurposing of a COX-1 human neuroimaging agent,  $^{11}\text{C}$ -PS13, for visualizing human OvCa tumors in subcutaneous and intraperitoneal xenograft mouse models. Clinical translation of this radiopharmaceutical for early detection of OvCa is warranted.

## DISCLOSURE

Amanda Boyle was supported by the CAMH Discovery Fund. Neil Vasdev was supported by the Azrieli Foundation, the Canada Research Chairs Program, the Canada Foundation for Innovation, and the Ontario Research Fund. Sami Zoghbi, Victor Pike, and Robert Innis were supported by the Intramural Research Program of the National Institutes of Health (NIMH; projects ZIA-MH002793, ZIA-MH002795, and ZIAMH002852). No other potential conflict of interest relevant to this article was reported.

## KEY POINTS

**QUESTION:** Can a COX-1-targeted neuro-PET imaging radiopharmaceutical be repurposed for the detection of OvCa?

**PERTINENT FINDINGS:** This study showed that  $^{11}\text{C}$ -PS13 could visualize OVCAR-3 OvCa tumors in subcutaneous and physiologically relevant intraperitoneal xenograft mouse models with excellent target specificity.

**IMPLICATIONS FOR PATIENT CARE:** The radiopharmaceutical  $^{11}\text{C}$ -PS13 may be rapidly translated for human PET imaging of OvCa.

## REFERENCES

- Torre LA, Trabert B, DeSantis CE, et al. Ovarian cancer statistics, 2018. *CA Cancer J Clin*. 2018;68:284–296.
- Park T, Lee S, Park S, et al. Value of [ $^{18}\text{F}$ ]FDG PET/CT in the detection of ovarian malignancy. *Nucl Med Mol Imaging*. 2015;49:42–51.
- Khiewvan B, Torigian DA, Emamzadehfard S, et al. An update on the role of PET/CT and PET/MRI in ovarian cancer. *Eur J Nucl Med Mol Imaging*. 2017;44:1079–1091.
- Antunes IF, van Waarde A, Dierckx RA, de Vries EG, Hospers GA, de Vries EF. Synthesis and evaluation of the estrogen receptor beta-selective radioligand 2-[ $^{18}\text{F}$ ]fluoro-6-(6-hydroxynaphthalen-2-yl)pyridin-3-ol: comparison with 16 $\alpha$ -[ $^{18}\text{F}$ ]fluoro-17 $\beta$ -estradiol. *J Nucl Med*. 2017;58:554–559.
- Makvandi M, Pantel A, Schwartz L, et al. A PET imaging agent for evaluating PARP-1 expression in ovarian cancer. *J Clin Invest*. 2018;128:2116–2126.
- Ocak M, Gillman AG, Bresee J, et al. Folate receptor-targeted multimodality imaging of ovarian cancer in a novel syngeneic mouse model. *Mol Pharm*. 2015;12:542–553.
- Tsuyoshi H, Morishita F, Orisaka M, Okazawa H, Yoshida Y.  $^{18}\text{F}$ -fluorothymidine PET is a potential predictive imaging biomarker of the response to gemcitabine-based chemotherapeutic treatment for recurrent ovarian cancer: preliminary results in three patients. *Clin Nucl Med*. 2013;38:560–563.
- Trencsényi G, Márián T, Lajtos I, et al. [ $^{18}\text{F}$ ]FDG, [ $^{18}\text{F}$ ]FLT, [ $^{18}\text{F}$ ]FAZA, and  $^{11}\text{C}$ -methionine are suitable tracers for the diagnosis and in vivo follow-up of the efficacy of chemotherapy by miniPET in both multidrug resistant and sensitive human gynecologic tumor xenografts. *BioMed Res Int*. 2014;2014:787365.
- Li F, Zhang Z, Cai J, et al. Primary preclinical and clinical evaluation of  $^{68}\text{Ga}$ -DOTA-TMVP1 as a novel VEGFR-3 PET imaging radiotracer in gynecological cancer. *Clin Cancer Res*. 2020;26:1318–1326.
- Sharma R, Valls PO, Inglese M, et al. [ $^{18}\text{F}$ ]fluciclatide PET as a biomarker of response to combination therapy of pazopanib and paclitaxel in platinum-resistant/refractory ovarian cancer. *Eur J Nucl Med Mol Imaging*. 2020;47:1239–1251.
- Beeghly-Fadiel A, Wilson AJ, Keene S, et al. Differential cyclooxygenase expression levels and survival associations in type I and type II ovarian tumors. *J Ovarian Res*. 2018;11:17.
- Wilson AJ, Fadare O, Beeghly-Fadiel A, et al. Aberrant over-expression of COX-1 intersects multiple pro-tumorigenic pathways in high-grade serous ovarian cancer. *Oncotarget*. 2015;6:21353–21368.
- Lau MT, Wong AS, Leung PC. Gonadotropins induce tumor cell migration and invasion by increasing cyclooxygenases expression and prostaglandin  $\text{E}_2$  production in human ovarian cancer cells. *Endocrinology*. 2010;151:2985–2993.
- Uddin MJ, Wilson AJ, Crews BC, et al. Discovery of furanone-based radiopharmaceuticals for diagnostic targeting of COX-1 in ovarian cancer. *ACS Omega*. 2019;4:9251–9261.
- Kim MJ, Shrestha SS, Cortes M, et al. Evaluation of two potent and selective PET radioligands to image COX-1 and COX-2 in rhesus monkeys. *J Nucl Med*. 2018;59:1907–1912.
- Kim M-J, Lee J-H, Juarez Anaya F, et al. First-in-human evaluation of [ $^{11}\text{C}$ ]PS13, a novel PET radioligand, to quantify cyclooxygenase-1 in brain. *Eur J Nucl Med Mol Imaging*. 2020;47:3143–3151.
- Singh P, Shrestha S, Cortes-Salva MY, et al. 3-substituted 1,5-diaryl-1 H-1,2,4-triazoles as prospective PET radioligands for imaging brain COX-1 in monkey. Part 1: synthesis and pharmacology. *ACS Chem Neurosci*. 2018;9:2610–2619.
- Shrestha S, Singh P, Cortes-Salva MY, et al. 3-substituted 1,5-diaryl-1 H-1,2,4-triazoles as prospective PET radioligands for imaging brain COX-1 in monkey. Part 2: selection and evaluation of [ $^{11}\text{C}$ ]PS13 for quantitative imaging. *ACS Chem Neurosci*. 2018;9:2620–2627.
- Wilson AA, Garcia A, Houle S, Vasdev N. Utility of commercial radiosynthetic modules in captive solvent [ $^{11}\text{C}$ ]-methylation reactions. *J Labelled Comp Radiochem*. 2009;52:490–492.
- Defrise M, Kinahan PE, Townsend DW, Michel C, Sibomana M, Newport DF. Exact and approximate rebinning algorithms for 3-D PET data. *IEEE Trans Med Imaging*. 1997;16:145–158.
- Moran MD, Wilson AA, Elmore CS, et al. Development of new carbon-11 labelled radiotracers for imaging GABA $_A$ - and GABA $_B$ -benzodiazepine receptors. *Bioorg Med Chem*. 2012;20:4482–4488.
- Pushpakom S, Iorio F, Eyers PA, et al. Drug repurposing: progress, challenges and recommendations. *Nat Rev Drug Discov*. 2019;18:41–58.
- Pannunzio A, Coluccia M. Cyclooxygenase-1 (COX-1) and COX-1 inhibitors in cancer: a review of oncology and medicinal chemistry literature. *Pharmaceuticals (Basel)*. 2018;11:101.